Kinetics of Triple Helix Formation in Semidilute Gelatin Solutions

Liang Guo,[†] Ralph H. Colby,*[,†] Charles P. Lusignan,[‡] and Thomas H. Whitesides[‡]

Materials Science and Engineering, The Pennsylvania State University, University Park, Pennsylvania 16802, and Imaging Materials and Media, R&D, Eastman Kodak Company, Rochester, New York 14650-2109

Received February 28, 2003; Revised Manuscript Received September 26, 2003

ABSTRACT: Using optical rotation to study the triple helix reversion of gelatin in aqueous solutions demonstrates that the reversion is a combination of first-order and second-order kinetic processes. On the basis of this observation, we propose a new two-step mechanism of triple helix formation in polypeptides, that leads to an expression distinct from the one obtained by Flory and Weaver. The rate-limiting step is formation of a two-stranded nucleus, which can be intramolecular (first order) or intermolecular (second order). The triple helix is formed by subsequent wrapping of a third strand onto this nucleus. We estimate the minimum stable helix length and the size of the loop at the end of an intramolecular helix from our kinetics analysis. The new two-step mechanism of triple helix formation is consistent with all existing literature data and allows prediction of concentration and temperature dependencies of helix formation rate.

Introduction

Gelatin is a biopolymer made from collagen through a hydrolysis process. The native conformation of collagen molecules is a triple helix formed by three individual molecular strands held together by interchain hydrogen bonding.[1] Gelatin, as denatured collagen, dissolves in water above its melting temperature and exists as flexible random coils[2] in solution. Upon cooling below the melting temperature, ordered structures of the gelatin molecules are re-formed. X-ray diffraction,[3] scattering,[4] and transmission electron microscopy[5] measurements strongly suggest that the reconstructed, ordered structures have the same conformation as collagen. In semidilute solutions, gelatin molecules highly interpenetrate each other and this poses topological difficulties for a complete coil−helix reversion to the collagen state. Gelatin molecules partially revert to the ordered triple helical collagen-like sequences, separated along the gelatin molecular contour by peptide residues in a disordered coil conformation. While the coil−helix reversion is predominantly intramolecular at very low concentrations, it becomes increasingly intermolecular in the semidilute regime and leads to gelation at concentrations above about 0.5 g/dL as a result of the formation of an infinite molecular network in the gelatin solution.[6]

The widespread applications of gelatin in food, pharmaceutical, and photographic industries are directly attributed to its coil−helix transition. Consequently, study of this coil−helix transition has attracted considerable research attention for over 50 years. The review by Rose[7] presents an outline of the research prior to 1977, and more investigations have been carried out over the past 25 years. Kinetics of the coil−helix transition has been studied extensively using techniques such as differential scanning calorimetry, polarimetry, scattering, and rheology to determine thermodynamic parameters, reversion rate, and helix fraction, as well as helix conformational properties.[2−30]

A fundamental question regarding the coil−helix transition is how fast this process proceeds and what are the effects of solution concentration and temperature. Flory and Weaver[10] studied the reversion rate in dilute rat-tail-tendon gelatin solutions and proposed a first-order kinetics with respect to concentration. They postulated a two-step renaturation process, with a single-chain intermediate that rapidly forms renatured triple helix. The Flory−Weaver renaturation process may be represented schematically as

$$\mathrm{C} \xrightarrow{k_1} \mathrm{I} \xrightarrow{k_2} (1/3)\,\mathrm{H} \tag{1}$$

where C, I, and H represent, respectively, the random coil, the intermediate, and the triple helix. The first step is much slower than the second step and, hence, is rate controlling. The rate of the Flory−Weaver renaturation process is given by the product of gelatin concentration, c, and the rate constant, k_1:[10]

$$k_1 = B \exp\left(\frac{-A}{kT\Delta T}\right) \tag{2}$$

where B and A are constants, T (in K) is the renaturation temperature, and $\Delta T \equiv T_m - T$ is the degree of undercooling, with T_m being the equilibrium melting temperature of the gelatin solution at the given concentration. For lime-processed ossein gelatin, T_m is about 35 °C for dilute solutions and increases to approximately 37 °C at a concentration of 10 g/dL.

While the first-order kinetic analysis agrees with experimental observations for dilute gelatin solutions,[10,15] it is contrary to the results obtained at moderately high concentrations where a concentration-dependent rate constant is usually reported.[12,15,23] Consequently, the Flory−Weaver mechanism is not valid in semidilute solutions. Several new mechanisms have been proposed for the renaturation kinetics. Drake and Veis[11] proposed that the first-order dependence on concentration of the renaturation process could result

* Corresponding author. E-mail: rhc@plmsc.psu.edu.
[†] The Pennsylvania State University.
[‡] Eastman Kodak Co.

10.1021/ma034264s CCC: $25.00
Published on Web 11/26/2003

from an "intramolecular reaction in which different segments of the same molecular chain must interact to form stable collagen-fold units." Harrington and Rao[15] adopted the idea of Drake and Veis for renaturation in dilute solutions and suggested that the rate-limiting step at high gelatin concentrations is the formation of a hydrogen-bonded nucleus composed of chain segments belonging to three separate molecules resulting in a third-order dependence on concentration. Eagland et al.[19] visualized the rate-determining step for dilute solutions as an initial formation of single turns of left-handed helix on a single chain, followed by a subsequent slow folding back of the chain upon itself twice, bringing the single helical turns into conjunction with one another. The triple helix is formed by the rapid "zipping up" of the chain segments contained in the loops. This scheme is intramolecular in nature and has a first-order concentration dependence.

All the above schemes propose either a first-order or third-order gelatin renaturation process. Harrington and Rao[15] suggested a combination of first- and third-order reversions for their concentration-dependent renaturation, despite an apparent combination of first- and second-order reversions seen in their data for gelatin solutions up to a concentration of 0.1 g/dL. Ter Meer and co-workers[23] observed a combination of first- and second-order renaturation for limed-bone gelatin solutions up to a concentration of 2 g/dL at 10 °C. In view of the discrepancies between the proposed mechanism and the experimental observations, a thorough study over wider concentration and temperature ranges is necessary. In the present paper, we present our experimental studies on the initial renaturation process of bovine-bone gelatin solutions at semidilute concentrations from 0.25 to 11.9 g/dL and over a temperature range from 3 to 30 °C, in an effort to elucidate the gelatin renaturation mechanism. *We find that a combination of first- and second-order kinetics applies and propose a new mechanism consistent with all observations.*

Experiment

In this work, experiments were performed with the same deionized lime-processed ossein gelatin (molecular weight 118 kDa, SKW Gelatin and Specialties) as used for a separate study of gelatin gelation,[6] without further purification. The only appreciable salt comes from a pH adjustment with NaOH which typically amounts to about 3000−3500 ppm sodium in the gelatin. All other anions and cations are less than 100 ppm. The solution pH is 5.7−5.8, significantly above the isoelectric point of 4.9. This gelatin contains 13.47% moisture by weight and the dry gelatin density is determined to be 1.45 g/cm^3 by measuring the weight of an aqueous gelatin solution of known concentration and volume. Aqueous gelatin solutions were prepared by swelling the gelatin in distilled, deionized water at room temperature for 1 h, followed by subsequent heating at 45 °C for another hour, under constant mild stirring. Concentration is on a dry gelatin weight basis and 0.2 g/dL Kathon biocide (Rohm and Haas) was added to the solutions. No pH adjustment was made to the gelatin solutions. The prepared gelatin solutions were stored in a refrigerator at 5 °C until use.

Gelatin is an optically active material in both the random coil and helix conformations but has more optical activity in the helix state. The polarization of an incident light beam passing through the gelatin sample rotates by an amount that depends on the beam wavelength and the optical activity. The optical rotation α (in degrees) measured at wavelength λ was normalized by the beam path length l (in decimeters) and the gelatin concentration c (in grams per deciliter) to yield the specific optical rotation

$$[\alpha]_\lambda = \frac{100\alpha}{lc} \tag{3}$$

The reverted fraction of triple helices in the renaturation process is related to the optical rotation change through a linear relationship between the optical rotation change and the fraction X of gelatin in the triple helix state[17a,21]

$$X = \frac{[\alpha]_\lambda - [\alpha]_\lambda^{\text{coil}}}{[\alpha]_\lambda^{\text{collagen}} - [\alpha]_\lambda^{\text{coil}}} \tag{4}$$

where $[\alpha]_\lambda$ is the measured specific optical rotation, $[\alpha]_\lambda^{\text{coil}}$ is the specific optical rotation if all the gelatin molecules are in the coil state, and $[\alpha]_\lambda^{\text{collagen}}$ is the specific optical rotation corresponding to complete renaturation (the native state of collagen). $[\alpha]_\lambda^{\text{coil}}$ has a nonzero value because the peptide chain (gelatin is a polypeptide) is chiral in the random coil state. Gelatin is levorotary, and its optical rotation by definition is negative.

The wavelength dependence of the specific optical rotation of collagen and gelatin solutions has been shown to follow the one-term Drude equation for $\lambda > 300$ nm[31]

$$[\alpha]_\lambda = D\frac{{\lambda_0}^2}{\lambda^2 - {\lambda_0}^2} \tag{5}$$

where D depends on the conformation of the protein, and λ_0 is the wavelength of the absorption maximum. This relation has been experimentally verified for collagen and gelatin solutions[24] in both the sol and gel states over a wide range of wavelengths, solution concentrations, and temperatures. The value of λ_0 for both partially renatured gelatin and collagen[24] is $\lambda_0 = 212$ nm, and the value of $[\alpha]_\lambda^{\text{collagen}}$ for limed ossein[24] is $[\alpha]_{436}^{\text{collagen}} = -800 \pm 10$. In this work, the optical rotation was measured at a wavelength of $\lambda = 632.8$ nm, and the corresponding specific optical rotation for collagen at this wavelength was calculated according to the Drude equation (eq 5) to be

$$[\alpha]_{632.8}^{\text{collagen}} = -327 \pm 5$$

The measured optical rotation of the gelatin used in this work in the coil state was $[\alpha]_{623.8}^{\text{coil}} = -120$ at 45 °C and reached −134.5 at 0 °C with a linear relationship to temperature change (see eq 6 below). The optical rotation in the collagen state, as calculated above, was used as a temperature independent parameter in this study.

The details of the polarimetry measurement with our custom-built instrument are described elsewhere.[6] In this work, a jacketed cylindrical brass cell, with an inner diameter of 2.5 mm and a path length of 100 mm, was used as the sample holder. The jacket is connected through a switching system to two water baths controlled at two temperatures, each with a stability of ±0.05 °C. Quenching is achieved by switching water flow from the two water baths. Water circulating in the cold water duct was maintained without passing through the jacket, prior to quenching, by using a separate switch to ensure that the water pumped into the jacket was at the right temperature at the start of quenching. Foamed rubber was used as thermal insulation to wrap the whole duct system. Temperature in the water baths and in the sample cell was calibrated with a thermocouple and it was found that the cell in quenching was able to reach the target temperature with an error 1.5% of the temperature drop in 25 s. Figure 1 shows the temperature response in the sample cell during quenches from 45 °C to various temperatures.

The gelatin solution was loaded into the sample cell and maintained at 45 °C for 1000 s to eliminate thermal history effects. Next, it was quenched to the desired low temperature to start the renaturation process. As shown in Figure 2 for a

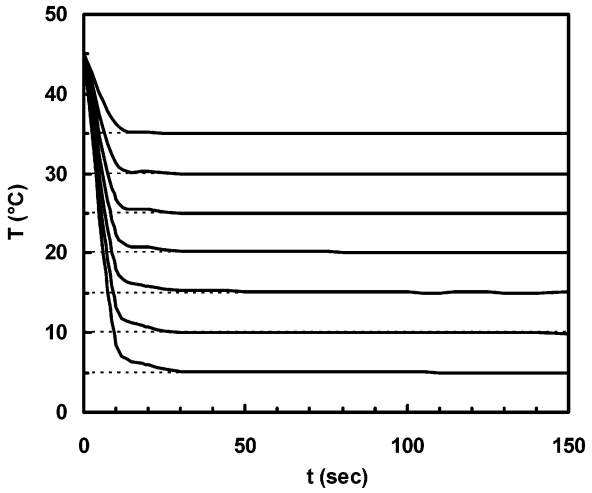

Figure 1. Temperature response in the brass sample cell on quenching to various temperatures, as measured with a thermocouple immersed in water inside the cell.

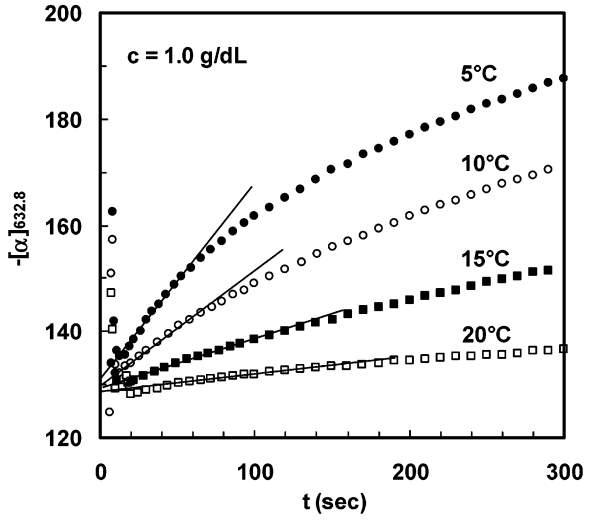

Figure 2. Optical rotation curves (at $\lambda = 632.8$ nm) after quenching from 45 °C to four different temperatures for a 1.0 g/dL gelatin solution.

1.0 g/dL gelatin solution quenched to 4 different temperatures (5, 10, 15, and 20 °C), the specific optical rotation is characterized by an initial jump with oscillations in the first 15 s from the original value of $[\alpha]_{632.8}^{coil} = -120°$ at 45 °C to a higher value around −130°, followed by a steady increase starting at about 20 s. The oscillations in the first 15 s are believed to be caused by the temperature gradient in the sample during the quench. The big jump of optical rotation in the first 15 s has a distinctively higher rate than that seen after 20 s and cannot be solely attributed to helix formation. Water volume changes by only 1% for a temperature drop from 45 to 5 °C and, thus, also cannot account for such a large initial jump in optical rotation (∼7% at 20 °C). Our interpretation is that gelatin chains in the coil state have a temperature-dependent optical rotation.

The optical rotation in the coil state at different temperatures is determined by extrapolating the slope in Figure 2 to a quench time of 10 s, and finding the actual temperature at that moment after quench (refer to Figure 1). The time of 10 s is selected based on the consideration that right after quench there is a fast drop as well as a large gradient of temperature within the sample cell, while too long after quench there is a significant amount of helix contribution to the optical rotation. Plotted in Figure 3 are the values of $[\alpha]_{632.8}$ vs the corresponding temperatures for gelatin solutions at several concentrations. The data points in filled symbols are

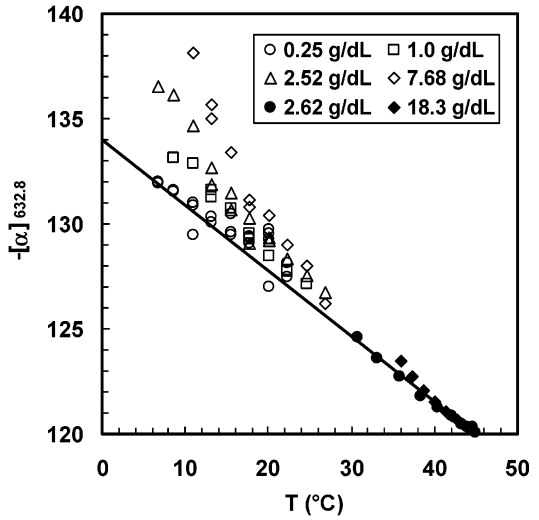

Figure 3. Optical rotation at 10 s after quench as a function of the actual temperature reached for gelatin solutions at several concentrations. Data points in filled symbols are for solutions slowly cooled from 45 °C with a rate of 0.5 K/min.

for gelatin solutions which are slowly cooled from 45 °C at a rate of 0.5 K/min. The lower boundary line of the data points has the minimum contribution from renatured helices and thus presents a close approximation of the optical rotation in the coil state. Data points at high gelatin concentrations and low temperatures deviate from the lower boundary line due to fast helix formation. The optical rotation in the coil state represented by the lower boundary line in Figure 3 can be described by a linear temperature dependence

$$[\alpha]_{632.8}^{coil} = 0.311T - 134 \tag{6}$$

where temperature T is in Celsius.

Results

The helical renaturation rate is directly related to the time-derivative of the optical rotation (eq 4)

$$\frac{dX}{dt} = -\psi\frac{d[\alpha]_{632.8}}{dt} \tag{7}$$

through a temperature-dependent factor:

$$\psi = \frac{1}{[\alpha]_{632.8}^{coil} - [\alpha]_{632.8}^{collagen}} \tag{8}$$

The slope of the optical rotation curve vs time is a direct measure of the helix renaturation rate. This slope is calculated from the optical rotation curves in Figure 2, starting at 20 s. For a quenching temperature close to the coil−helix transition temperature (∼35 °C), the renaturation rate is low, and a longer time is required for proper slope calculation, to minimize the residual error introduced by the temperature gradient in the first 15 s. Figure 4 shows the initial rate of optical rotation change obtained for gelatin solutions at concentrations from 0.25 to 11.9 g/dL quenched to temperatures in a range from 3 to 30 °C. The rate decreases with temperature but increases with gelatin concentration. However, at low temperatures and high gelatin concentrations, the rate decreases with concentration. This effect is believed to be caused by the limitation of the heat transfer rate of the brass cell. Since helix formation is an exothermic process, any deficiency in heat transfer will raise the sample temperature and decrease the

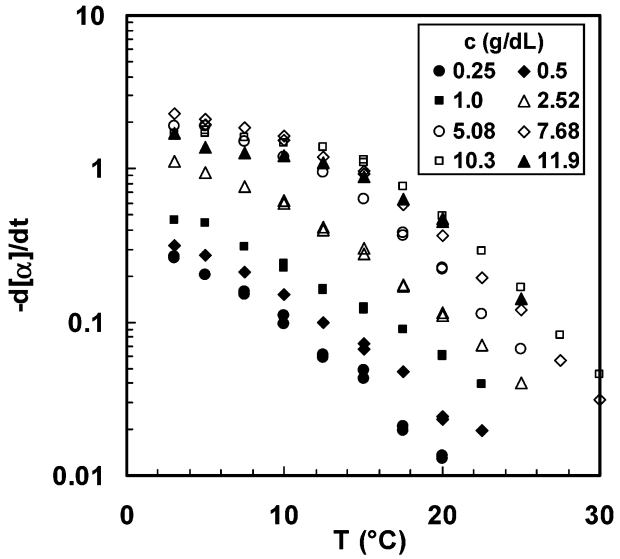

Figure 4. Temperature dependence of the initial rate of change in optical rotation for gelatin solutions at different concentrations.

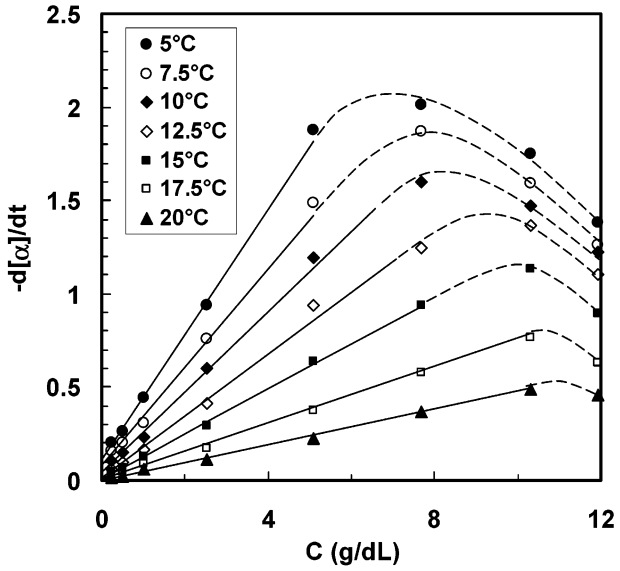

Figure 5. Concentration dependence of the initial rate of change in optical rotation at different quench temperatures, showing a constant slope at low concentrations and a nonzero intercept. The solid lines are the fit, and the dashed lines are for visual guidance.

helix reversion rate. This effect is more obvious when the data are plotted against concentration as shown in Figure 5. At concentrations below 5.08 g/dL, the rate shows a linear dependence on concentration for temperatures in the range ~5−20 °C. The solid, straight lines are the result of a weighted least-squares fit with more weight given to lower concentrations. The concentration dependence of the fit lines can be described as

$$-\frac{\mathrm{d}[\alpha]}{\mathrm{d}t} = K'_1 + c_0 K'_2 \tag{9}$$

where c_0 is the initial gelatin concentration, K'_1 and K'_2 are the intercept and slope of the lines that depend on temperature only. This result is also consistent with the experimental observation of Ter Meer and co-workers.[23] Next, we demonstrate that the form of eq 9 indicates a combination of first- and second-order helix reversions.

Equations for the first- and second-order helix reversions can be written, respectively, as

$$\frac{\mathrm{d}[H]_1}{\mathrm{d}t} = [C]K_1 \tag{10}$$

and

$$\frac{\mathrm{d}[H]_2}{\mathrm{d}t} = [C]^2 K_2 \tag{11}$$

where $[H]_i$ is the moles of helices per unit volume created by the reversion process of order i, $[C]$ is the moles per unit volume of amino residues in the flexible coil segments, K_i is the rate constant for the reversion process of order i, and the subscripts 1 and 2 denote the first- and second-order reversions. The helix fraction X is related to $[H]_1$ and $[H]_2$ through the helix lengths l_1^* and l_2^*, which are assumed to be the minimum stable helix lengths for each reversion process

$$c_0 X = M_l(l_1^*[H]_1 + l_2^*[H]_2) \tag{12}$$

where M_l is the molecular weight per unit triple helix length. The initial rate of change of optical rotation is

$$-\frac{\mathrm{d}[\alpha]}{\mathrm{d}t} = \frac{1}{\psi}\frac{\mathrm{d}X}{\mathrm{d}t} = \frac{M_l}{c_0\psi}\left(l_1^*\frac{\mathrm{d}[H]_1}{\mathrm{d}t} + l_2^*\frac{\mathrm{d}[H]_2}{\mathrm{d}t}\right)$$

$$= \frac{M_l}{c_0\psi}(l_1^*[C]K_1 + l_2^*[C]^2K_2) \tag{13}$$

Since the coil concentration $[C] = (1 - X)c_0/M_{\mathrm{res}} \approx c_0/M_{\mathrm{res}}$ for very small X at the initial stage of helix reversion, where M_{res} (= 92 D)[32] is the molecular weight per amino acid residue, eq 13 simplifies to

$$-\frac{\mathrm{d}[\alpha]}{\mathrm{d}t} = \frac{1}{\psi l_{\mathrm{res}}}\left(l_1^*K_1 + c_0\frac{l_2^*K_2}{M_{\mathrm{res}}}\right) \tag{14}$$

where l_{res} (= 2.86 Å)[33] is the length per residue. This equation has the same concentration dependence as our experimental observations as described by eq 9. Hence, the experimental results in Figure 5 represent a combination of first- and second-order reversions. A solely first-order reversion would require the fit lines in Figure 5 to be horizontal, and an exclusively second-order reversion would require the lines to pass through the origin. Any order higher than 2 would lead to a nonlinear dependency on concentration and, therefore, an upward curvature in Figure 5.

Discussion

The formation of a triple helix is completed through two steps: nucleation and wrapping. The nucleation step involves a positive-activation energy (demonstrated below) and is much slower than the wrapping step (a negative energy is associated with the wrapping step). The slow nucleation process is rate-limiting so it determines the reaction order.

Table 1 shows the possible critical nucleus structures for first-order, second-order, and third-order reversions, involving critical nuclei with one, two, or three strands. Flory and Weaver[10] proposed a critical nucleus involving a single strand for which only first-order kinetics is possible. Clearly, the single strand nucleus cannot

Table 1. Possible Critical Nucleus Structures

	1st order	2nd order	3rd order
1 strand			
2 strands			
3 strands			

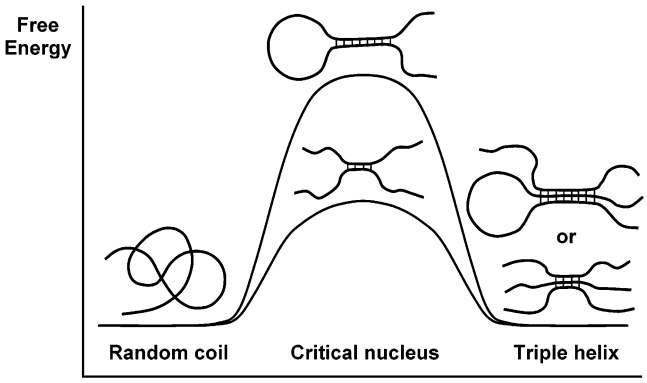

Figure 6. Schematic of triple helix formation of the two-strand nucleation mechanism. Single-looped helices are formed in dilute solutions, nonlooped helices are found in concentrated solutions, while single-looped helices coexist with nonlooped helices in semidilute solutions.

explain our observation of a contribution from second-order kinetics. The three-strand nucleus proposed by Harrington and Rao[15] could be formed by one chain (first order), two chains (second order), or three chains (third order). Harrington and Rao correctly asserted that the most common of these would be the third-order reversion, because the loops required for first- and second-order reversions of three-strand nuclei cost free energy. The fact that we see no evidence for third-order kinetics (nor is there any evidence in the literature) suggests that the critical nucleus does not involve three strands.

Thus, the only possible mechanism is the initiation of a two-strand nucleus. The formation of a triple helix is realized in *two* steps: (1) slow initiation of a nucleus composed of two helical strands winding together and (2) rapid subsequent wrapping of another coil segment around the nucleus to form a triple helix. Triple helices exceeding a critical length remain stable, but shorter ones remelt immediately after their formation.

In the first-order reversion, the two strands of the nucleus are from a single chain with a loop. The triple helix either contains two loops, if the third wrapping coil is from the same chain, or has one loop, if the wrapping coil is from another chain. The single-looped helices are more likely to be formed, so, single-looped helices are predominantly created by the first-order reversion.

Therefore, the two-strand nucleation mechanism is more appropriate in describing the coil−helix reversion dependence on concentration: dominant, single-looped helices in the dilute regime developed to the coexistence of single-looped and nonlooped helices in the semidilute regime and, finally, to dominant nonlooped helices for concentrated solutions. The triple helix formation process of the two-strand nucleation mechanism is schematically shown in Figure 6 for both the looped and nonlooped helices.

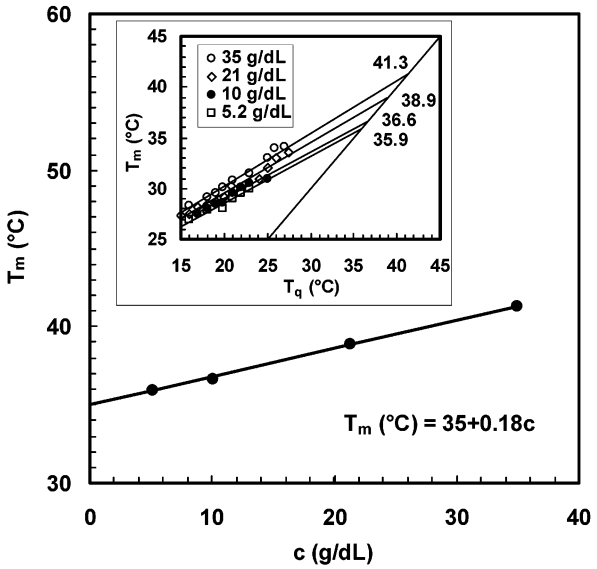

Figure 7. Reanalysis of the literature DSC data[20] for the concentration dependence of the equilibrium melting temperature T_m of gelatin solutions. T_q in the inset is the quench temperature in the DSC measurements and the measured data are extrapolated to the $T_m = T_q$ line to get the equilibrium melting temperature, at each concentration.

The minimum stable helix length can be derived in a similar way to the treatment of Flory and Weaver.[10] The free energy of formation of a triple helix of length l at the quench temperature T is given by

$$\Delta G = l(\Delta H - T\Delta S) + 2\sigma_e + \epsilon u_b \qquad (15)$$

where ΔH (<0) and ΔS (<0) are the enthalpy and entropy changes per helix length when the helix is formed, σ_e (>0) is the interfacial free energy at the two ends of the helix, u_b (>0) is the bending free energy stored in the loop, and the parameter ϵ takes a value of zero for a nonlooped triple helix and a value of 1 for a single-looped helix. The minimum stable helix length l^* is found by setting eq 15 equal to zero:

$$l^* = -\frac{2\sigma_e + \epsilon u_b}{\Delta H - T\Delta S} \qquad (16)$$

The approximation $\Delta S = \Delta H/T_m$ may be derived from the fact that $\Delta H - T\Delta S = 0$ at the equilibrium melting temperature T_m. By denoting the undercooling $\Delta T \equiv T_m - T$, the minimum stable helix length can be rewritten as

$$l^* = -\frac{2\sigma_e + \epsilon u_b}{\Delta H}\frac{T_m}{\Delta T} \qquad (17)$$

It is seen that the minimum stable helix length is inversely proportional to the relative undercooling $\Delta T/T_m$. The critical helix length l_1^* of the first-order reversion is longer than the critical helix length l_2^* of the second-order reversion, because there is no loop energy ($\epsilon = 0$) in the second-order reversion.

The concentration dependence of T_m for lime-processed ossein gelatin is plotted in Figure 7 through reanalyzing the available literature DSC data[20] (shown as the inset of Figure 7). A simple linear approximation

can be used for the concentration dependence of the melting temperature

$$T_m^0(°C) = 35 + 0.18c \tag{18}$$

By using the Kratky−Porod model,[34] the loop-bending free energy can be calculated with the following integration along the contour of the loop modeled as a wormlike chain[35]

$$u_b = \frac{1}{2} l_p kT \int_0^L \left(\frac{\partial \boldsymbol{u}(s)}{\partial s}\right)^2 ds \tag{19}$$

where l_p is the persistence length (= 20 ± 3Å for gelatin),[36] and $\boldsymbol{u}(s)$ is the unit vector tangent to the contour at length s. Assuming a circular end loop of radius R_l, the bending free energy is simplified as

$$u_b = \frac{1}{2} l_p kT \int_0^L \frac{1}{R_l^2} ds = \frac{1}{2} l_p kT \int_0^{2\pi} \frac{1}{R_l^2} R_l \, d\theta = \frac{\pi l_p kT}{R_l} \tag{20}$$

Equation 20 indicates that the bending free energy is proportional to the absolute temperature (entropic) but inversely proportional to the loop size, with the assumption that l_p and R_l are not temperature dependent.

As discussed above, the formation of a triple helix of the minimum stable length l^* is realized through nucleation and subsequent wrapping. The rate-limiting process is nucleation. *The rate constant for triple helix reversion is effectively given by the rate of nucleation*

$$K = B \exp(-E/kT) \tag{21}$$

where B is the collision frequency factor, and E is the free energy for the creation of the nucleus. The energy E, which is positive, is the activation energy for nucleation. Through assigning ΔH_1 and ΔS_1 as the enthalpy and entropy per unit nucleus length, and σ_{e1} as the nucleus end surface energy, the total activation energy for the reversion of a triple helix of the critical length l^* can be written

$$E = 2\sigma_{e1} + \epsilon u_b + (\Delta H_1 - T\Delta S_1) l^* \tag{22}$$

Since two of the three chain strands are involved in forming the critical nucleus, the entropy ΔS_1 and end surface energy σ_{e1} of the nucleus are $^2/_3$ of those of the full triple helix. The enthalpy ΔH_1 for nucleus creation, however, cannot simply be assumed to be $^2/_3$ of that of the full triple helix. Assume that the fusion enthalpy is solely a result of the energy of hydrogen-bonding interactions between chain strands. As shown in Figure 8, there are three mutual interactions between the three chain strands in a triple helix. The oxygen and hydrogen atoms bonding together are in a plane perpendicular to the helix axis. In a nucleus, two of the three interactions responsible for bonding the third wrapping coil segment reorganize to form a new interaction between the two strands of the nucleus. Owing to topological constraints, the reorganization of interactions will lead to two out-of-plane hydrogen-bonding pairs (the bonding plane is not perpendicular to the nucleus axis), or one in-plane and one out-of-plane bonding pairs. Since the out-of-plane bonding is weaker than the in-plane bonding, the enthalpy associated with nucleus creation is less than $^2/_3$, but more than $^1/_3$, of that for the triple helix (see Figure 8). A more accurate estimation of the nucleus

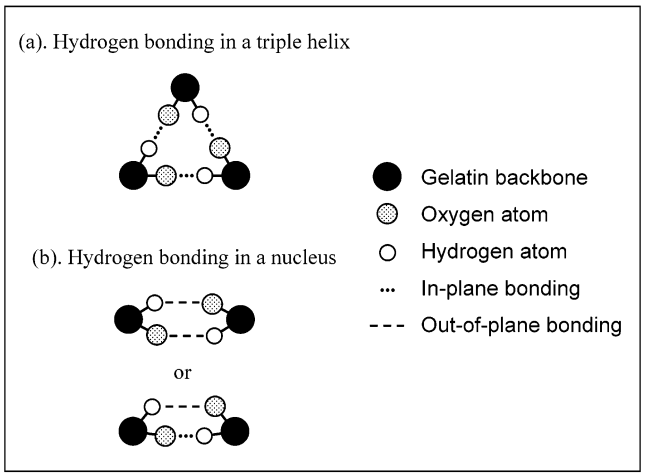

Figure 8. Schematic comparison in a cross-sectional view of hydrogen bonding in a triple helix and a two-stranded nucleus.

enthalpy requires knowledge of the topological and hydrogen-bonding features of the nucleus. The enthalpy, entropy, and end-surface energies of the nucleus are therefore given as

$$\Delta H_1 = \alpha \Delta H \quad \text{with} \quad {}^1/_3 < \alpha < {}^2/_3 \tag{23}$$

$$\Delta S_1 = \frac{2}{3}\Delta S \tag{24}$$

$$\sigma_{e1} = \frac{2}{3}\sigma_e \tag{25}$$

Substituting the energy estimates and the critical helix length into eq 22 and using the relations $\Delta S = \Delta H/T_m$ and $\Delta T \equiv T_m - T$, the total activation energy for the formation of the triple helix can be simplified as

$$E = \frac{\epsilon}{3} u_b + \left(\frac{2}{3} - \alpha\right)(2\sigma_e + \epsilon u_b)\frac{T_m}{\Delta T} > 0 \tag{26}$$

Since the overall energy for a triple helix formation at the critical length is zero (eq 15), the positive energy E for the nucleation process implies a negative energy for the wrapping process. Therefore, the nucleation process is thermodynamically unfavorable and slow, while the wrapping process is thermodynamically favored and fast (see Figure 6). This is consistent with the assumption that the nucleation process is slow and rate limiting.

With the activation energy given by eq 26 the rate constant is derived as

$$\begin{aligned} K &= B \exp\left(-\frac{\epsilon}{3}\frac{u_b}{kT}\right) \exp\left(-\left(\frac{2}{3} - \alpha\right)\frac{2\sigma_e + \epsilon u_b}{kT}\frac{T_m}{\Delta T}\right) \\ &= B \exp(-A_1) \exp\left(-A_2 \frac{T_m}{\Delta T}\right) \\ &= B' \exp\left(-A_2 \frac{T_m}{\Delta T}\right) \end{aligned} \tag{27}$$

where the two positive parameters $A_1 = \epsilon u_b/3kT$ and $A_2 = (2-3\alpha)(2\sigma_e + \epsilon u_b)/3kT$ are assumed to be temperature-independent constants (because $u_b \propto kT$, eq 20, and assuming an entropic $\sigma_e \propto kT$). Equation 27 indicates that the rate constant K depends only on the end surface energy σ_e and loop bending energy u_b but not on the enthalpy ΔH and entropy ΔS at a given

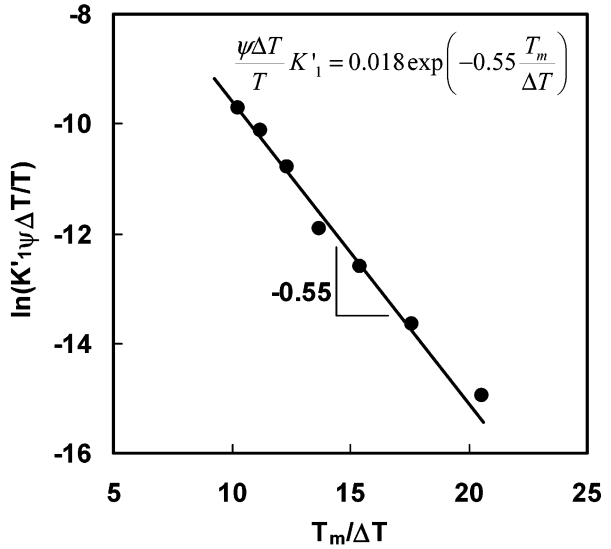

Figure 9. Temperature dependence of the first-order rate constant plotted in the form suggested by eq 30.

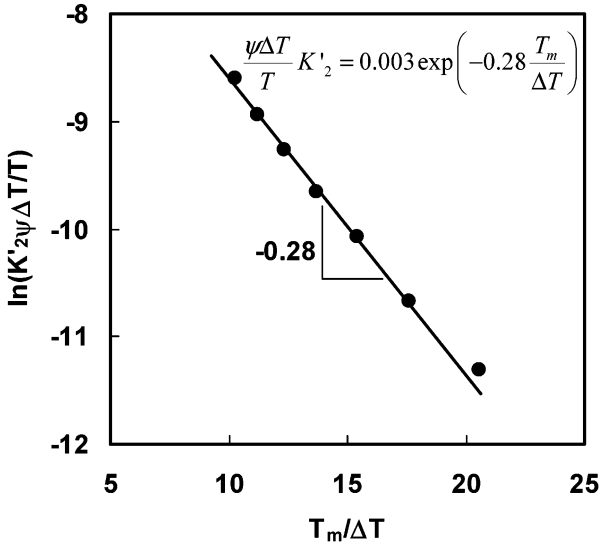

Figure 10. Temperature dependence of the second-order rate constant plotted in the form suggested by eq 31.

quench temperature. The thermodynamic quantity ΔH or ΔS (recall that $\Delta S = \Delta H/T_m$) only affects the minimum stable helix length l^* (eq 17).

Comparison of eqs 9 and 14 leads to the following expressions that relate the rate constants with the intercept and slope of the fit lines in Figure 5 (with $\epsilon =$ 1 and 0 for the first- and second-order reversions, respectively)

$$K'_1 = \frac{l_1^* K_1}{\psi l_{res}} = \frac{1}{\psi l_{res}} \frac{2\sigma_e + u_b}{-\Delta H} \frac{T_m}{\Delta T} K_1 \quad \text{for} \quad \epsilon = 1 \tag{28}$$

$$K'_2 = \frac{l_2^* K_2}{\psi l_{res} M_{res}} = \frac{1}{\psi l_{res} M_{res}} \frac{2\sigma_e}{-\Delta H} \frac{T_m}{\Delta T} K_2 \quad \text{for} \quad \epsilon = 0 \tag{29}$$

The intercept K'_1 in eq 28 corresponds to zero concentration and, hence, the single-looped, first-order reversion, so eq 17 with $\epsilon = 1$ is used for l_1^*. The slope K'_2 in eq 29 comes mainly from the contribution of the second-order reversion, thus a value of $\epsilon = 0$ for nonlooped helices is used for l_2^*. Combining eqs 27−29 leads to the following relations

$$K'_1 = B_1 \frac{kTT_m}{-\psi\Delta H\Delta T} \exp\left(-\left(\frac{2}{3} - \alpha\right)\frac{2\sigma_e + u_b}{kT}\frac{T_m}{\Delta T}\right) \tag{30}$$

$$K'_2 = B_2 \frac{kTT_m}{-\psi\Delta H\Delta T} \exp\left(-\left(\frac{2}{3} - \alpha\right)\frac{2\sigma_e}{kT}\frac{T_m}{\Delta T}\right) \tag{31}$$

where B_1 and B_2 are the combined constants. It should be pointed out that eqs 30 and 31 are only valid for the low concentration limit because of the concentration-dependent T_m. Plotting the normalized intercept $K'_1\psi\Delta T/T$ and slope $K'_2\psi\Delta T/T$ logarithmically against $T_m/\Delta T$ should give two straight lines, whose slopes determine the value of the end surface energy σ_e and loop bending free energy u_b. Figures 9 and 10 are such plots corresponding to low concentration (with $T_m = 35$ °C) in a quench temperature range from 5 to 17.5 °C. The two straight lines have slopes of −0.55 and −0.28, respectively, leading to the value of the end surface energy and end loop energy for $\alpha = 0.59$ (see the Appendix for the α value determination by optical rotation modeling)

$$\sigma_e = \frac{0.42}{2 - 3\alpha} kT = 1.8kT \tag{32}$$

$$u_b = \frac{0.81}{2 - 3\alpha} kT = 3.5kT \tag{33}$$

The minimum stable lengths of the first-order, single-looped and second-order, nonlooped helices are calculated as

$$l_1^* = -\frac{1.65}{2 - 3\alpha}\frac{kTT_m}{\Delta H\Delta T} = -7.2\frac{kTT_m}{\Delta H\Delta T} \tag{34}$$

and

$$l_2^* = -\frac{0.84}{2 - 3\alpha}\frac{kTT_m}{\Delta H\Delta T} = -3.7\frac{kTT_m}{\Delta H\Delta T} \tag{35}$$

The end loop radius is deduced as

$$R_l = \frac{\pi kT}{u_b} l_p \approx \frac{\pi}{3.5} l_p = 18\text{Å} \tag{36}$$

With the helix melting enthalpy[18] $-\Delta H \simeq 11$ cal/g of helix, or equivalently ∼1100 (cal/Å)/mol of helices, the critical helix length, at a quench temperature of $T =$ 20 °C and a melting temperature of $T_m = 35$ °C, for the single-looped and nonlooped triple helices is calculated as 72 and 37 Å, respectively. In Figure 11, the critical helix lengths at the early stage of helix conversion for the single-looped helices of the first-order reversion and the nonlooped helices of the second-order reversion are plotted against quench temperature for the melting temperature $T_m = 35$ °C.

In addition to the helix lengthening effects, complications like network formation also prevent our simple model from describing long time data. When a network with high connectivity is formed, the coil segments connecting the junction zones (formed by the second-order helices) are stretched at high helix fraction. This stretching leads to entropy loss of the coil segments, and hence, an additional energy comparable to the loop bending free energy of the first-order helices should be

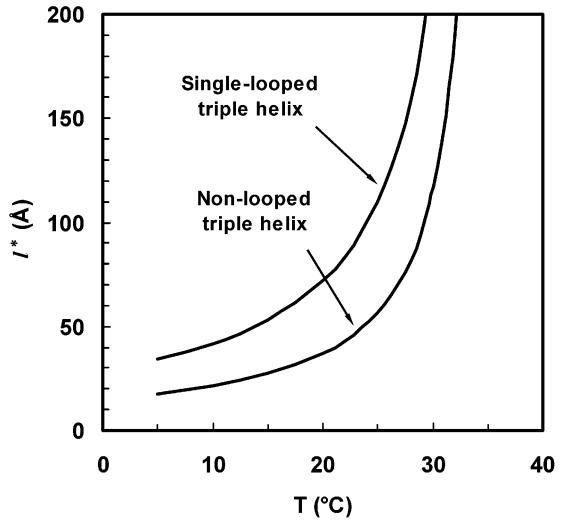

Figure 11. Critical helix length of single-looped and non-looped helices at the early stage of quenching as a function of quench temperature for an equilibrium melting temperature $T_m = 35$ °C.

included in calculating the second-order helix length. However, this extra energy only affects coil−helix reversion at long times.

In addition to the concentration dependence of the helix reversion kinetics, temperature is shown to also affect helix reversion order. From eqs 10 and 11, it follows that

$$\frac{d[H]_2}{dt}\Big/\frac{d[H]_1}{dt} = [C]\frac{K_2}{K_1} = [C]\frac{B_2'}{B_1'}\exp\left(\left(\frac{2}{3}-\alpha\right)\frac{u_b}{kT}\frac{T_m}{\Delta T}\right) = [C]\frac{B_2'}{B_1'}\exp\left(0.27\frac{T_m}{\Delta T}\right) \quad (37)$$

Equation 37 indicates that the second-order reversion becomes dominant when concentration is raised, because the coil concentration $[C]$ is simply proportional to the initial concentration, a result consistent with Figure 5. Another implication of eq 37 is that for the same concentration, the ratio of second-order reversion to first-order reversion increases as temperature is raised (smaller $\Delta T \equiv T_m - T$), indicating that a larger portion of the total converted helix is intermolecular at higher temperatures. This result is consistent with our separate study[6] where lower critical helix fraction X_{gel} is found at higher temperatures (where longer helices are formed) for a gelatin solution of a given concentration to reach the gel point. The smaller number density of helices required to reach the gel point at higher temperatures demands more intermolecular helix formation as temperature is raised.

Conclusions

We develop a simple model for the kinetics of the thermoreversible triple helix formation, and derive temperature and concentration dependences that are markedly different from the predictions of the Flory and Weaver model. A combination of first- and second-order reversions was observed for the concentration dependence of gelatin triple helix renaturation. This combined reversion mechanism is interpreted as the formation of single-looped triple helices in dilute solutions and non-looped triple helices in concentrated solutions. The triple helix end surface energy and loop bending energy are estimated to be $1.8kT$ and $3.5kT$, respectively. The helix length of the single-looped helices is roughly twice that of the nonlooped helices, and both are inversely proportional to undercooling. The helix end loop radius is estimated as 18 Å, comparable to the persistence length of gelatin, 20 Å.

Acknowledgment. We thank Eastman Kodak Company for financial support of this research and Andrew Howe, Roland Koestner, and Phil Rose for many technical discussions.

VI. Appendix

The fits to eqs 30 and 31 in Figures 9 and 10 lead to the following relations

$$\frac{\psi\Delta T}{T}K'_1 = 0.018\exp\left(-\frac{0.55T_m}{\Delta T}\right) \quad (38)$$

$$\frac{\psi\Delta T}{T}K'_2 = 0.003\exp\left(-\frac{0.28T_m}{\Delta T}\right) \quad (39)$$

The optical rotation at the initial stage (helix fraction $X \approx 0$) has been shown by our experiments to take the following format

$$-\frac{d[\alpha]}{dt} = K'_1 + c_0K'_2 \quad (40)$$

In terms of helix fraction X (eq 7), eq 40 is equivalent to

$$\frac{dX}{dt} = -\psi\frac{d[\alpha]}{dt} = 0.018\frac{T}{\Delta T}\exp\left(-\frac{0.55T_m}{\Delta T}\right) + 0.003\frac{T}{\Delta T}\exp\left(-\frac{0.28T_m}{\Delta T}\right)c_0 \quad (41)$$

where the first term accounts for the first-order reversion, and the second term for the second-order reversion. Here we have neglected a changing T_m in the prefactors before the two exponentials as a result of the very small error introduced (refer to eqs 30 and 31).

Equation 41 is only valid for the initial stage of helix reversion ($X \approx 0$). At longer times in the early stage, the helix reversion equation should be

$$\frac{dX}{dt} = \frac{dX_1}{dt} + \frac{dX_2}{dt} = 0.018\frac{T}{\Delta T}\exp\left(-\frac{0.55T_m}{\Delta T}\right)(1 - X_1 - X_2 - \xi X_1 - \zeta X_2) + 0.003\frac{T}{\Delta T}\exp\left(-\frac{0.28T_m}{\Delta T}\right)c_0(1 - X_1 - X_2 - \xi X_1 - \zeta X_2)^2 \quad (42)$$

where X_1 and X_2 are the helix fractions created by the first- and second-order reversions. In eq 42, the term $(1 - X_1 - X_2 - \xi X_1 - \zeta X_2)$ is the coil fraction being capable of making new nuclei of both the first- and second-order reversions. We assume that when the first-order single-looped helices are formed, the coil segments contained in the loop *are not* capable of making new nuclei. This coil fraction is proportional to the fraction

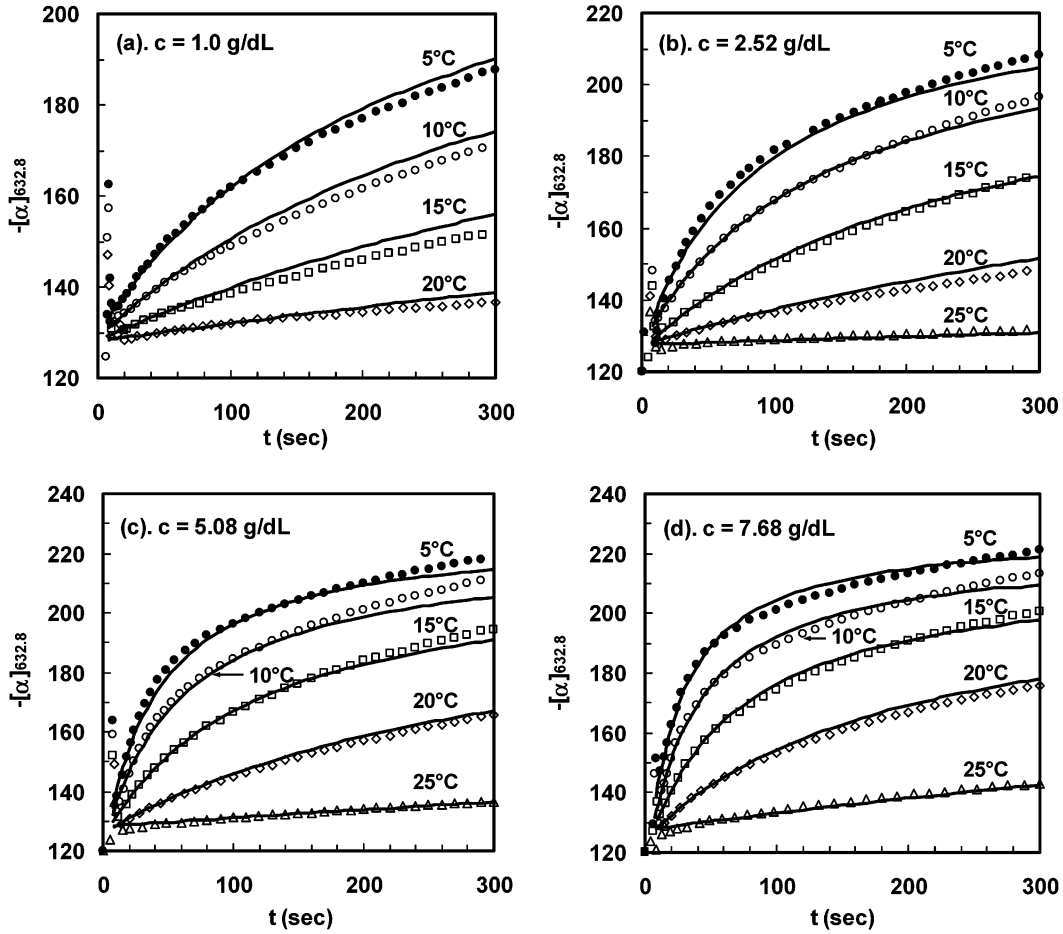

Figure 12. Comparison of the prediction of the combined mechanism of first- and second-order reversions with experimental optical rotation for four gelatin concentrations quenched to different temperatures.

of the single-looped helices ξX_1, with $\xi = 2\pi R_l/3l_1^*$, a temperature-dependent constant. For the second-order helix reversion, a local network of several molecules will be formed with the helices acting as the junction zones. The coil segments connected by the junction zones have hindered mobility and *are not* capable of making new nuclei. This hindrance comes from the fact that a molecule is involved in several junction zones, and the hindrance should be proportional to the fraction of the molecule being involved in the helices. Thus, the coil fraction not capable of making new nuclei as a result of the second-order helix formation should be proportional to the fraction of second-order helices ζX_2, with ζ being a universal constant valid for all concentrations and temperatures. It is expected that $\zeta > 1$, because if half of the gelatin molecule has been involved in making the second-order helices, the remaining coil segments do not have enough length to make new helices if the existing helices are evenly distributed along the molecule.

Equation 42 can be simplified as a set of two equations

$$\frac{dX_1}{dt} = a(1 - \theta X_1 - \varphi X_2)$$
$$\frac{dX_2}{dt} = b(1 - \theta X_1 - \varphi X_2)^2 \tag{43}$$

by denoting

$$a = 0.018\frac{T}{\Delta T}\exp\left(-\frac{0.55T_m}{\Delta T}\right)$$
$$b = 0.003\frac{T}{\Delta T}\exp\left(-\frac{0.28T_m}{\Delta T}\right)c_0$$
$$\theta = 1 + \xi \tag{44}$$
$$\varphi = 1 + \zeta$$

The solution for this set of equations with the initial condition $X_1(0) = X_2(0) = 0$ is solved as

$$X_1 = -\frac{a^2\theta t}{b\varphi} + \frac{a}{b\varphi}\ln\left(\frac{(a\theta + b\varphi)\exp(a\theta t) - b\varphi}{a\theta}\right)$$
$$X_2 = \frac{1}{\varphi}\left(1 + \frac{a^2\theta^2 t}{b\varphi} - \frac{a\theta}{(a\theta + b\varphi)\exp(a\theta t) - b\varphi} - \frac{a\theta}{b\varphi}\ln\left(\frac{(a\theta + b\varphi)\exp(a\theta t) - b\varphi}{a\theta}\right)\right) \tag{45}$$

The total helix fraction is then

$$X = X_1 + X_2$$
$$= \frac{1}{\varphi} + \frac{a^2\theta(\theta - \varphi)}{b\varphi^2}t - \frac{1}{\varphi}\frac{a\theta}{(a\theta + b\varphi)\exp(a\theta t) - b\varphi} - \frac{a(\theta - \varphi)}{b\varphi^2}\ln\left(\frac{(a\theta + b\varphi)\exp(a\theta t) - b\varphi}{a\theta}\right) \tag{46}$$

with θ given by

$$\theta = 1 + \xi = 1 + \frac{2\pi R_l}{3l_1^*} = 1 + 4(2 - 3\alpha)^2 \frac{\Delta H \Delta T l_p}{kTT_m} \quad (47)$$

The optical rotation, according to eq 4, is given by

$$[\alpha] = [\alpha]^{coil} + ([\alpha]^{collagen} - [\alpha]^{coil})X \quad (48)$$

The value of $[\alpha]^{collagen}$ in eq 48 is -327 and the value of $[\alpha]^{coil}$ is given by eq 6. With the literature enthalpy value $-\Delta H \simeq 11$ cal/g of helix, based on DSC and optical rotation measurements,[18] and the persistence length value of a gelatin coil $l_p \simeq 20 \pm 3$ Å,[36] eq 48 fits to the experimental optical rotation data very well for the universal fitting parameters $\alpha = 0.59 \pm 0.01$ and $\varphi = 2.37 \pm 0.03$ (or $\zeta = 1.37$) for gelatin solutions at the concentrations of 1.0, 2.52, 5.08, and 7.68 g/dL in the temperature range ~5−25 °C, as shown in Figure 12. The melting temperature T_m for each concentration is calculated using eq 18. All the fit lines have been shifted horizontally for 10 s, in accordance with the temperature response retardation in the sample cell (see Figure 1), and vertically by a value equivalent to the initial jump in optical rotation at 10 s after quench (this is equivalent to shifting the origin of coordinates). A value of $\zeta = 1.37$ ($\varphi = 1 + \zeta = 2.37$) implies that at most ~45% of the gelatin can be converted to triple helix through the nucleation process. Reversions higher than ~45% require a contribution from helix lengthening. Thus, a fast helix growth region due to the nucleation process will terminate before a helix fraction of ~0.45 is reached at low temperatures; thereafter, a slow helix growth region caused by helix lengthening continues, and this is often observed in the literature data. At high temperatures, the lengthening rate is comparable to the very low nucleation rate, and there is often no obvious separation between fast and slow helix growth regions.

References and Notes

(1) Ramachandran, G. N.; Kartha, G. *Nature (London)* **1954**, *174*, 269; *Nature (London)* **1955**, *176*, 593.

(2) Boedtker, H.; Doty, P. *J. Phys. Chem.* **1954**, *58*, 968−983.

(3) Pezron, I.; Djabourov, M.; Bosio, L.; Leblond, J. *J. Polym. Sci., Part B: Polym. Phys.* **1990**, *28*, 1823−1839.

(4) Pezron, I.; Herning, T.; Djabourov, M.; Leblond, J. In *Physical Networks*; Burchard, W.; Ross-Murphy, S. B.; Eds.; Elsevier: Amsterdam, 1990.

(5) Djabourov, M.; Bonnet, N.; Kaplan, H.; Favard, N.; Favard, P.; Lechaire, J. P.; Maillard, M. *J. Phys. II* **1993**, *3*, 611−624.

(6) Guo, L.; Colby, R. H.; Lusignan, C. P.; Howe, A. M. *Macromolecules* **2003**, *36*, 10009.

(7) Rose, P. I. In *The Theory of the Photographic Process*, 4th ed.; James, T. H., Ed.; Macmillan: New York, 1977.

(8) Djabourov, M. *Contemp. Phys.* **1988**, *29*, 273−297.

(9) Ferry, J. D.; Eldridge, J. E. *J. Phys. Chem.* **1949**, *53*, 184.

(10) Flory, P. J.; Weaver, E. S. *J. Am. Chem. Soc.* **1960**, *82*, 4518−4525.

(11) Drake, M. P.; Veis, A. *Biochemistry* **1964**, *3*, 135.

(12) Piez, K. A.; Carrillo, A. L. *Biochemistry* **1964**, *3*, 908.

(13) Beier, G.; Engel, J. *Biochemistry* **1966**, *5*, 2744−2755.

(14) Petrie, S. E. B.; Becker, R. In *Analytical Calorimetry*; Porter, R. S., Johnson, J. E., Eds.; Plenum Press: New York, 1970; Vol. 2.

(15) Harrington, W. F.; Rao, N. V. *Biochemistry* **1970**, *9*, 3714−3724.

(16) Harrington, W. F.; Karr, G. M. *Biochemistry* **1970**, *9*, 3725−3733.

(17) Hauschka, P. V.; Harrington, W. F. *Biochemistry* **1970**, *9*, 3734−3745. Hauschka, P. V.; Harrington, W. F. *Biochemistry* **1970**, *9*, 3745−3754. Hauschka, P. V.; Harrington, W. F. *Biochemistry* **1970**, *9*, 3754−3763.

(18) Macsuga, D. D. *Biopolymers* **1972**, *11*, 2521−2532.

(19) Eagland, D.; Pilling, G.; Wheeler, R. G. *Faraday Discuss. Chem. Soc.* **1974**, *57*, 181−200.

(20) Godard, P.; Biebuyck, J. J.; Daumerie, M.; Naveau, H.; Mercier, J. P. *J. Polym. Sci.: Polym. Phys. Ed.* **1978**, *16*, 1817−1828.

(21) Djabourov, M.; Papon, P. *Polymer* **1983**, *24*, 537.

(22) Chatellier, J. Y.; Durand, D.; Emery, J. R. *Int. J. Biol. Macromol.* **1985**, *7*, 311−314.

(23) Ter Meer, H. U.; Lips, A.; Busnel, J.-P. In *Physical Networks, Polymers and Gels*; Burchard, W.; Ross-Murphy, S. B., Eds.; Elsevier: Amsterdam, 1990.

(24) Djabourov, M.; Leblond, J.; Papon, P. *J. Phys. (Paris)* **1988**, *49*, 319−332 and *J. Phys. (Paris)* **1988**, *49*, 333−343.

(25) Burjanadze, T. V.; Bezhitadze, M. O. *Biopolymers* **1992**, *32*, 951−956.

(26) Michon, C.; Cuvelier, G.; Relkin, P.; Launay, B. *Int. J. Biol. Macromol.* **1997**, *20*, 259−264.

(27) Bohidar, H. B.; Jena, S. S. *J. Chem. Phys.* **1993**, *98*, 8970−8977.

(28) Bohidar, H. B.; Jena, S. S. *J. Chem. Phys.* **1994**, *100*, 6888−6895.

(29) Cuppo, F.; Venuti, M.; Cesàro, A. *Int. J. Biol. Macromol.* **2001**, *28*, 331−341.

(30) Gillmor, J. R.; Connelly, R. W.; Colby, R. H.; Tan, J. S. *J. Polym. Sci., Part B: Polym. Phys.* **1999**, *37*, 2287−2295.

(31) Von Hippel, P. H.; Wong, K. Y. *Biochemistry* **1963**, *2*, 1399.

(32) Eastoe, J. E. *Biochem. J.* **1955**, *61*, 589.

(33) Astbury, W. T. *Proc. Intern. Soc. Leather Trades Chem.* **1940**, *24*, 69.

(34) Kratky, O.; Porod, G. *Recl. Trav. Chim. Pays-Bas* **1949**, *68*, 1106.

(35) Doi, M.; Edwards, S. F. *The Theory of Polymer Dynamics*; Oxford University Press: New York, 1986.

(36) Pezron, I.; Djabourov, M.; Leblond, J. *Polymer* **1991**, *32*, 3201.

MA034264S